Journal of Materials Science: Materials in Electronics (2018) 29:7002–7014
https://doi.org/10.1007/s10854-018-8687-y

Enhanced photocatalytic degradation of rhodamine B, methylene blue and 4-nitrophenol under visible light irradiation using TiO_2/MgZnAl layered double hydroxide

Guoqing Zhao[1] · Jiao Zou[1] · Caifeng Li[1] · Jingang Yu[1] · Xinyu Jiang[1] · Yijian Zheng[1] · Wenjihao Hu[1,2] · Feipeng Jiao[1]

Received: 30 December 2017 / Accepted: 25 January 2018 / Published online: 13 February 2018
© Springer Science+Business Media, LLC, part of Springer Nature 2018

Abstract
Series of new TiO_2/MgZnAl layered double hydroxide (TiO_2/LDH) composites with different molar ratio of metals (Mg:Zn:Al) and a certain amount of recombined TiO_2 were successfully prepared by co-precipitation method. The prepared products were characterized by X-ray diffraction, Fourier transform infrared spectroscopy, scanning electron microscopy, N_2 adsorption–desorption measurements, X-ray photoelectron spectroscopy and UV–Vis diffuse reflectance spectroscopy. Rhodamine B (10 mg/L), methylene blue (10 mg/L) and 4-nitrophenol (4 mg/L) were used as model organic compounds for evaluation of the photocatalytic performance of the as-prepared photocatalysts under visible light irradiation. Results indicated that TiO_2/LDH composites (Mg:Zn:Al equals to 1:3:1) showed the highest photocatalytic activity and degraded 93.73, 85.88 and 89.33% of rhodamine B, methylene blue, and 4-nitrophenol in 9.0, 8.0 and 4.0 h, respectively. By comparison, the composites exhibited superior photocatalytic activity compared to P25 catalysts. The enhanced photocatalytic activity of the TiO_2/LDH composites mainly attributed to the efficient separation of photoinduced electrons and holes. Superoxide radicals and holes were the major active species. What's more, the as-prepared photocatalysts exhibited remarkable stability and reusability. Besides, the possible degradation mechanism of rhodamine B, methylene blue and 4-nitrophenol also were proposed in this paper. This work provides an effective way to prepare series of LDH-based photocatalysts.

1 Introduction

Nowadays, an increasing number of organic pollutants containing of phenolic compound derivatives, textile dyes, volatile organic compounds, antibiotic medicines, and herbicide derivatives responsible for environmental and water pollution are discovered [1–3]. Among these, textile dyes and phenolic compound derivatives are considered as the most difficult to decompose due to their special chemical structure and stability [4–6]. These organic pollutants are environmental killers to human's health and aquatic organisms because most of them are considered as carcinogenic and high toxic pollutants [7, 8]. Many efforts are being made to explore easy and economical technologies for wastewater pollutants treatment [9–15]. However, the obtained results were not very satisfactory. Hence, it is necessary to develop an environment-friendly and efficient approach to organic pollutants removal in wastewater treatment.

Advanced oxidation processes have been proved to be one of the promising recommended technologies for refractory and toxic organic pollutant removal from wastewater [16–18]. As one of the technologies, visible light driven photocatalysis technology offers a low-cost and green pathway that has widely application for complete removal of wastewater pollutants such as toxic dyes and other hazardous organic compounds from the effluents. In this regard, the visible light driven photocatalysis have received more and more attention for wastewater pollutant treatment in recent years [4, 19]. Besides, the visible light as an ideal source is a

Electronic supplementary material The online version of this article (https://doi.org/10.1007/s10854-018-8687-y) contains supplementary material, which is available to authorized users.

✉ Wenjihao Hu
huwenjihaoluke@126.com

✉ Feipeng Jiao
jiaofp@163.com

[1] School of Chemistry and Chemical Engineering, Central South University, Changsha 410083, People's Republic of China

[2] Donadeo Innovation Central for Engineering, Department of Chemical and Materials Engineering, University of Alberta, Edmonton T6G 1H9, Canada

clean energy for the aliment of a green atmosphere and cost effective process [20]. In order to achieve the high degradation rate of organic wastewater pollutants, it is important to exploit such visible light active photocatalytic materials.

Thankfully, semiconductor-based photocatalysis is an ideal chemical process for organic pollutants degradation, due to its cost-effectiveness and satisfactory catalytic efficiency [21–23]. Aiming at these views, mounts of novel nanostructure materials have been developed recently. Against this backdrop, novel nanostructured materials have been developed greatly to meet these environmental challenges.

Titanium dioxide (TiO_2), as an excellent photocatalysis, is one of the most widely accepted and fundamental photocatalytic materials owing to its chemical stability, nontoxicity, low prices, high photocatalytic activity, etc [24, 25]. However, single TiO_2 nanoparticles only work under ultraviolet light irradiation for its wide band gap [26–28]. So, many efforts about how to obtain the narrow band gap of modified TiO_2 have been tried in recent two decades [26, 29]. Khanchandani et al. developed a series of visible light driven photocatalysts (TiO_2/CuS, TiO_2@rGO, SiO_2@TiO_2, Au/TiO_2), and these photocatalysts showed excellent photocatalytic activity in the degradation of organic wastewater pollutants compared with single unmodified TiO_2 [30–32].

Layered double hydroxides (LDH), as typical 2D-nanostructured anionic clays, are widely used in the catalysis, adsorption, electrochemistry, and biotechnology [33, 34]. As multifunctional materials, the LDH composites include brucite-like hydroxide sheets, where some suitable groups can be incorporated. Their chemical composition are usually expressed by a general formula $[M_{1-x}^{2+}M_x^{3+}(OH)_2]^{x+}(A^{n-})_{x/n}\cdot mH_2O$, where M^{2+} is a bivalent cation such as Mn^{2+}, Zn^{2+}, Ni^{2+}, Ca^{2+} and Fe^{2+}; M^{3+} is a divalent cation such as Fe^{3+}, Ti^{3+}, Al^{3+} and Cr^{3+}; A^{n-} represents the interlayer anions such as NO_3^-, OH^-, CO_3^{2-} and other various organic anions which balance the positive charges on the layers; x is calculated by the equations $M^{3+}/(M^{2+} + M^{3+})$ [34–37]. Multiphases of LDHs which can be fabricated by the hydrothermal methods or ion-exchange processes have been studied for many years because of its potential uses [34]. Ternary layered double hydroxides with magnesium, zinc and aluminum in the laminate have been widely used as photocatalysts for its high photodegradation rate of organic wastewater pollutants [38–40]. TiO_2 and LDH are synthesized into a composited state in order to improve the photocatalytic activity through their common interaction under the visible light irradiation.

From the previous survey of the literature, there are several published articles about the organic wastewater pollutants degradation by the TiO_2/MgZnAl layered double hydroxides with different Mg/Zn/Al molar ratio and the fixed mass of TiO_2 nanoparticles. Meanwhile, the aimed photocatalysts were prepared by conventional co-precipitation of magnesium, zinc and aluminum salts from uniform solution and TiO_2 nanoparticles. The rhodamine B, methylene blue and 4-nitrophenol (Fig. 1) are chosen as model organic pollutants to assess the photocatalytic degradation activity of TiO_2/MgZnAl layered double hydroxides composites. Furthermore, the possible photocatalytic degradation mechanism of rhodamine B, methylene blue and 4-nitrophenol by the composites was put forward.

2 Experimental

2.1 Reagents and materials

$Mg(NO_3)_2\cdot 6H_2O$ and $Al(NO_3)_3\cdot 9H_2O$ were purchased from Fengchuan Chem. Co., Ltd. (Tianjin, China). $Zn(NO_3)_2\cdot 6H_2O$ was provided by Xilong Chem. Co., Ltd. (Guangdong, China). NaOH was supplied by Sinopharm Chem. Co., Ltd. (Shanghai, China), and titanium dioxide nanoparticles (P25) with a specific area of about 50 m^2/g and an average particle size of 10–15 nm was provided by Sinopharm Chemical Reagent Co., Ltd. Rhodamine B ($C_{28}H_{31}ClN_2O_3$) was purchased from Tianjin Kemiou Chemical Reagent Co., Ltd. Methylene blue ($C_{16}H_{18}ClN_3S\cdot 3H_2O$)

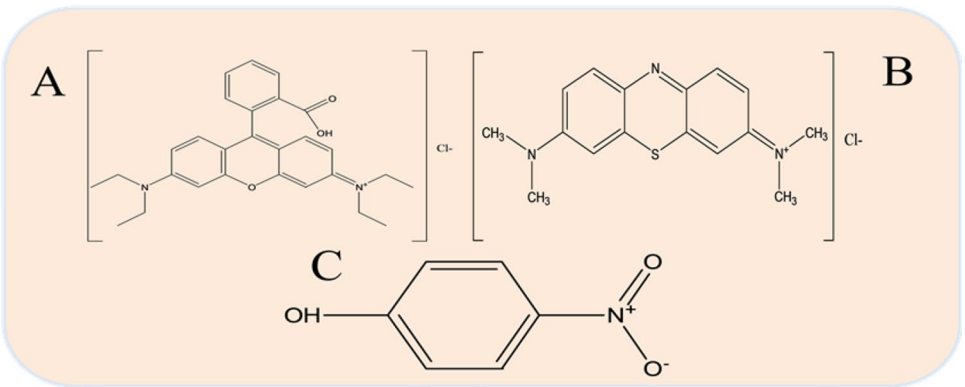

Fig. 1 The structure of target degradation, **a** rhodamine B; **b** methylene blue; **c** 4-nitrophenol

was supplied by Tianjin Chemical Reagent Research Institute Co., Ltd. and 4-nitrophenol ($C_6H_5NO_3$) was obtained from Sinopharm Chemical Reagent Co., Ltd. All reagents are analytical grade and those were used as received without further purification. All solutions were prepared with high purity distilled water.

2.2 Preparations of TiO_2/MgZnAl layered double hydroxides composites

Prior to TiO_2/MgZnAl layered double hydroxides composites synthesis, the TiO_2 was pre-treated based on the reported literature [41]. Briefly, 1.5 g P25 was dispersed in 10 M 20 mL of NaOH aqueous solution and placed into a Teflon-lined stainless autoclave. And then the autoclave was heated at 200 °C for 6 h. Afterwards, the autoclave was cooled down to the room temperature. Then, the presulfided TiO_2 nanoparticles were washed with 0.1 M HCl aqueous solution, deionized water and ethanol for several times, and then this obtained product was dried at 60 °C for overnight.

A series of TiO_2/MgZnAl layered double hydroxides composites were synthesized by fixing the Mg:Zn:Al molar ratio at 1:1:1, 1:1:2, 1:1:3 and 1:b:1 (b was 2–8). In a typical synthesis, a certain quality of $Mg(NO_3)_2{\cdot}6H_2O$, $Zn(NO_3)_2{\cdot}6H_2O$, $Al(NO_3)_3{\cdot}9H_2O$ and 50 mg of TiO_2 nanoparticles were dispersed in 200 mL of water by ultrasonic dispersion for 30 min. And then, adjusting the pH of the mixture to the range of 8–9 with 2 M NaOH solution, stirring the mixture for another 1 h after the reaction process was finished. After that, making the mixture solvents located in the oven vacuum at 60 °C for 24 h, then filtrating and washing in turn the resulted slurry by distilled water and ethanol for 6–8 times. Finally, the resulted solid was dried at 60 °C for overnight. The obtained photocatalysts were marked as TiO_2/LDH composites (TiO_2/LDH-111, TiO_2/LDH-112, TiO_2/LDH-113 and TiO_2/LDH-1b1, b was 2–8).

2.3 Characterization of photocatalysts

The crystallinity and phase analysis of the prepared TiO_2/LDH composites were detected by a Bruker D8 Advance X-ray diffractometer at the following parameters: Cu Kα radiation, λ = 1.5406 Å, 40 KV, 40 mA, and all the surveys were obtained in the 2θ extent of 10° and 80° at room temperature. The surface morphology of as-prepared products was evaluated by scanning electron microscopy (SEM), which was conducted by TESCAN MIRA3 LMU microscope. Fourier transform infrared (FT-IR) spectra were recorded using an AVATAR 360 spectrometer (Nicolet instrument Corporation, America) in the 4000–400 cm^{-1}. The surface chemical composition of the products was detected by X-ray photoelectron spectroscopy (XPS, PHI Quantera SXM, ULVAC-PHI, Japan), The Brunauer-Emmett-Teller (BET) surface areas and pore size distributions of photocatalysts were determined by Nitrogen adsorption isotherms under the following conditions: 77 K, 8 h outgas, and 100 °C in advance treatment. Additionally, the related pore diameter was calculated from the desorption branches using the Barrett–Joyner–Halenda (BJH) method, and pore volumes were estimated from the absorbed amount at a relative pressure of 0.90. The optical properties were evaluated by measuring the UV–Vis absorption spectrum of the as-prepared sample powders, which recorded by a spectrophotometer (Schimadzu 2401 spectrophotometer).

2.4 Measurements of catalytic performance

The photocatalytic performance of the as-prepared TiO_2/LDH composites was evaluated by the degradation of the model wastewater rhodamine B, methylene blue and 4-nitrophenol simulation solution in a photochemical reactor (YM-GHX-V, Yuming Instrument Co., Ltd., Shanghai, China). A 500 W xenon lamp worked as UV light source with a 400 nm cutoff filter (< 400 nm). Typically, 50 mg of prepared catalysts were added into 50 mL of rhodamine B, methylene blue and 4-nitrophenol aqueous solution with a concentration of 10, 10 and 4 mg/L, respectively. At first, the suspension including above mixture materials was constantly stirred for 1.0 h in dark to reach the adsorption–desorption equilibrium. In the meantime, the temperature of the photochemical reactor was kept at 25 °C with the help of circulating water during the experiment. Then, turning on the visible light, 3 mL of suspension was sucked out every 1 h and filtered immediately to be analyzed using a UV–Vis spectrophotometer (UV-9600) at 554, 664, and 317.5 nm, respectively. Because of the possible self-degradation of model organic simulation wastewater, the blank experiment was studied under the identical reaction conditions in the preliminary experiments.

3 Results and discussion

3.1 Characterization of the TiO_2/LDH composites

3.1.1 XRD

The XRD patterns of the pure TiO_2 and TiO_2/LDH composites were shown in Fig. 2. All the prepared samples had similar patterns, which proved a mixture of the anatase and rutile phases of TiO_2 existed. As for Fig. 2a, the diffraction peaks at $2\theta = 25.3°$, 37.7°, 47.9°, 53.8°, 62.6° and 74.9° can be ascribed to (1 0 1), (0 0 4), (2 0 0), (1 0 5), (2 0 4) and (2 1 2) reflection of anatase TiO_2 (JCPDS 21-1272), respectively. Moreover, the patterns also clearly showed peaks of rutile TiO_2, namely, the peaks at $2\theta = 27.8°$, 35.9°, 54.9° and

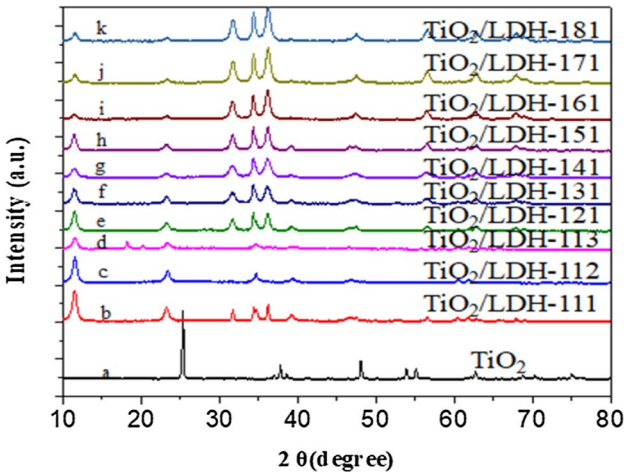

Fig. 2 XRD patterns of the TiO_2 (*a*), TiO_2/LDH-111 (*b*), TiO_2/LDH-112 (*c*), TiO_2/LDH-113 (*d*), TiO_2/LDH-121 (*e*), TiO_2/LDH-131 (*f*), TiO_2/LDH-141 (*g*), TiO_2/LDH-151 (*h*), TiO_2/LDH-161 (*i*), TiO_2/LDH-171 (*j*), and TiO_2/LDH-181 (*k*) composites

68.8° can be ascribed to (1 1 0), (1 0 1), (2 1 1) and (3 0 1) reflection of rutile TiO_2 (JCPDS 21-1276), respectively [42, 43]. Furthermore, the X-ray diffraction patterns of TO_2/LDH composites were shown in Fig. 2b–k. From Fig. 2, all the curves have the peak (003 (11.2°), 006 (23.5°), 009 (35.1°), 010 (61.8°)) of LDHs except the curve (a), and all the patterns of the samples have the typical peaks of TiO_2 [44]. The introduce of TiO_2 nanoparticles on the surface of the photocatalysts fabricated a hybrid and disordered compound structure, bringing on broad and weak diffraction peaks d(003) [45]. Seeing the Fig. 2b–k carefully, the different Mg/Zn/Al molar ratio also can impact the crystal, which may be due to the arrangement of different metal atoms.

3.1.2 SEM

The SEM analysis of the samples P25, TiO_2, and TiO_2/LDH composites were presented in Fig. 3. Figure 3a shows the micrograph of the untreated P25 had unordered spherical particles and a mixture of anatase and rutile in shape was appeared in the P25 nanoparticles, with a diameter of 300–700 nm. However, through alkali treatment, the surface of the TiO_2 particles becomes rougher compared with that of the original particles (Fig. 3b) and produce a large specific surface area (Table 1), which increased the active surface of the particles [46]. Furthermore, the original TiO_2 particles (alkali treated P25) are destroyed and the micrograph of TiO_2 exhibits like-lamellae nanosheets stacked. The rough

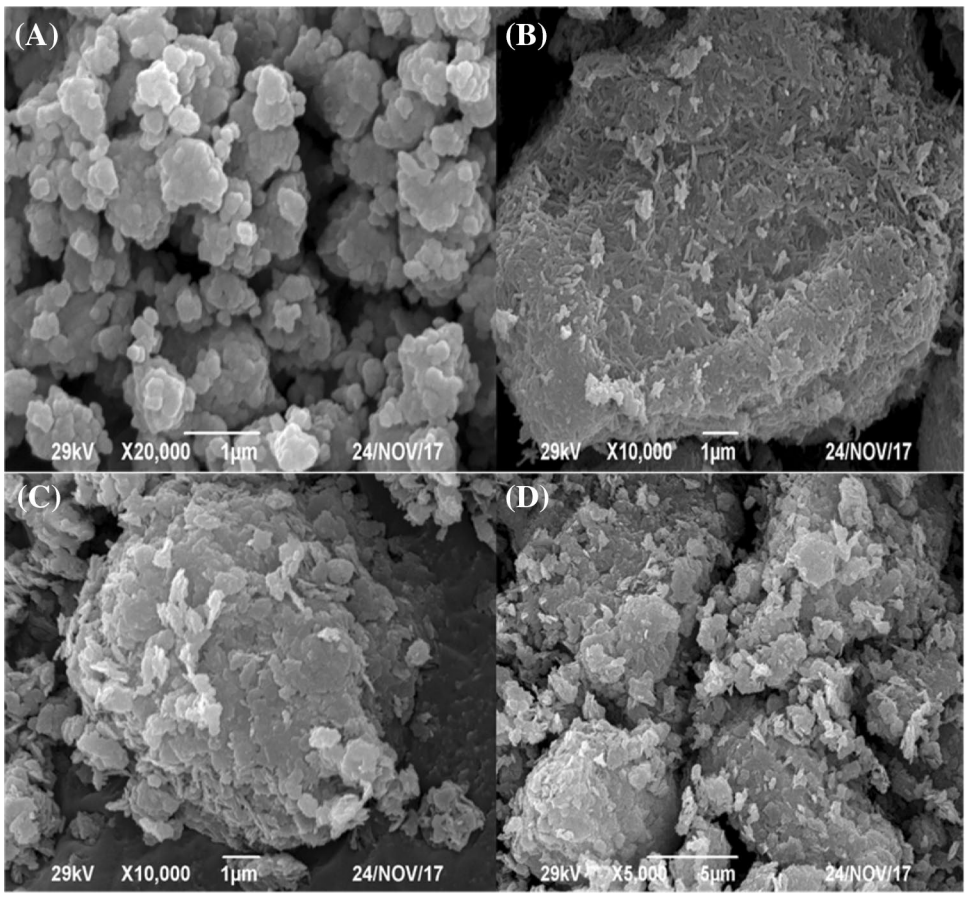

Fig. 3 SEM images of the P25 (1μ m) (**a**), TiO_2 (1μ m) (**b**), TiO_2/LDH-131 (1μ m) (**c**), and TiO_2/LDH-131 (5μ m) composites (**d**)

Table 1 The physico-chemical properties of the materials

Catalyst	Pore diameter (nm)	Pore volume (m^3)	Surface area (m^3/g)
TiO_2	9.960	0.166	33.425
TiO_2/LDH-131	14.330	0.436	60.827

surface of the stacked TiO_2 nanoparticles also provides high-energy location site for the nucleation and growth of LDH nanosheets (Fig. 3c). After assembly of stacked TiO_2 nanoparticles on the surface of LDH nanosheets, the heterostructures enhanced their coarseness. Under the present synthetic conditions, TiO_2 particles were tightly coated on the surface of layer double hydroxides via above hydrothermal methods, and then TiO_2 particles were uniformly formed on the surface of layered double hydroxides.

3.1.3 FT-IR

The FT-IR spectra (Fig. 4) of TiO_2/LDH composites were analyzed and compared with P25, TiO_2, and TiO_2/LDH-131 composites including hydroxyl species, carboxylic species, and epoxy species etc. Typically, Fig. 4a shows the FT-IR spectra of pure P25 particles. For pure P25 particles, the main peaks at 400–700 cm^{-1} are assigned to the stretching vibrations of Ti–O–Ti and Ti–O in particles crystals, while the other wide speaks at 1630 and 3420–3500 cm^{-1} correspond to –OH and physically-adsorbed water, respectively, which corresponding to the previous work [42]. As for Fig. 4b, the stretching vibration absorption at nearly 1630 cm^{-1} was enhanced, proving that the vibration of structure OH groups was improved by the sodium hydroxide solution. Figure 4c displays the infrared spectra of the TiO_2/LDH-131 composites. It showed broad absorption bands at around 3500 and 1633 cm^{-1}, which was considered as the OH stretching vibration of hydroxyl groups, water molecules in the interlayer, and physically adsorbed water [37, 40]. The M–O and O–M–O (M = Mg, Zn, Al, Ti) vibration bands appeared in the 400–800 cm^{-1} region [47–49]. Besides, the broad observed at nearly 1360 cm^{-1} was due to the stretching vibrations of CO_3^{2-}. The FT-IR results confirmed the aimed composites had been synthesized.

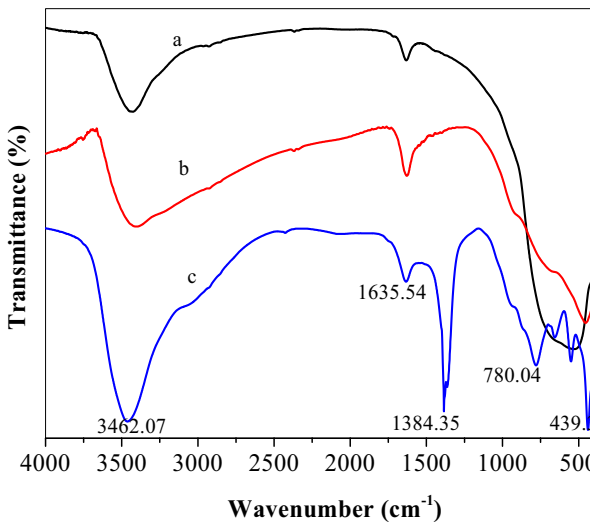

Fig. 4 FT-IR spectra of the P25 (*a*), TiO_2 (*b*), and TiO_2/LDH-131 composites (*c*)

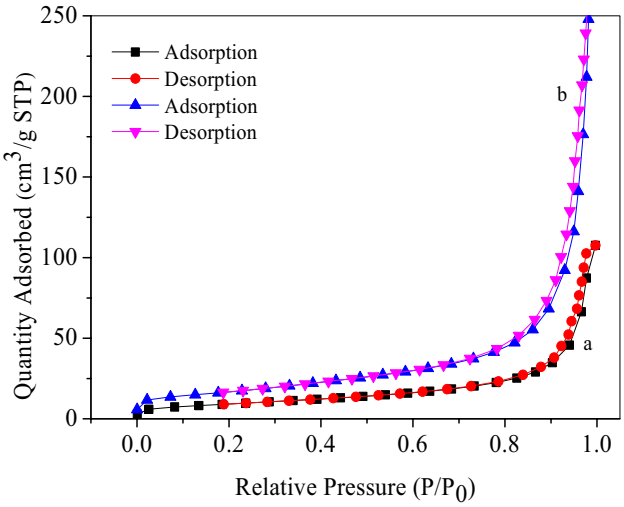

Fig. 5 The N_2 adsorption–desorption isotherm curve of (*a*) TiO_2 and (*b*) TiO_2/LDH-131 composites

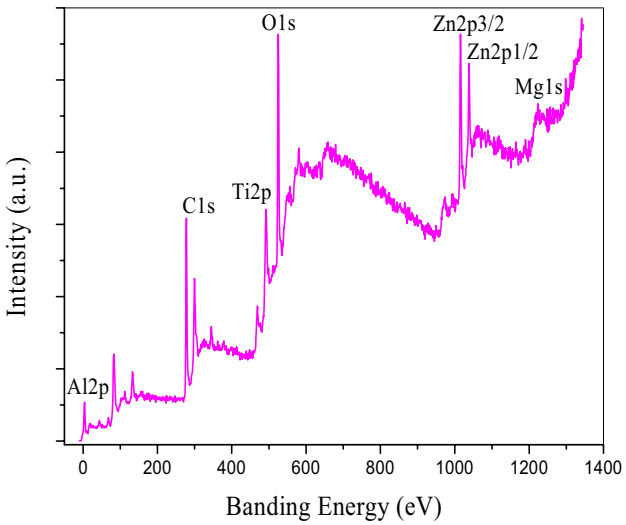

Fig. 6 XPS scan spectrum of TiO_2/LDH-131 composites

3.1.4 BET

N_2 adsorption–desorption measurements were performed to investigate the porosity of the as-prepared TiO_2 and TiO_2/LDH-131 composites. Figure 5 shows that all the photocatalysts exhibited a typical type-III isotherm according to the classification of the international Union of Pure and Applied Chemistry (IUPAC), indicating the mesoporous characteristics. The N_2 adsorbed quantity increased slowly with the increasing of relative pressure, reflecting the adsorbent–adsorbate interactions were relatively week. Apparently, the mesoporous TiO_2/LDH-131 composites have a higher specific surface area than pure TiO_2 nanoparticples, and the composites still remain the mesoporous structure. Table 1 presents the detailed information of the samples including BET surface area, pore volume, and average pore size. The TiO_2/LDH-131 composites have a high specific BET surface area of up to 6 0.827 m^2/g with an average pore size of 14.330 nm.

3.1.5 XPS

XPS was further applied to study the surface elemental compositions of the as-prepared TiO_2/LDH-131 composites. The full survey spectrum of the samples was shown in Fig. 6. As found in Fig. 6, the full survey spectrum of the samples suggested that the catalysts were composed of Mg, Zn, Al, Ti, O, and C elements. The signal of C was due to contamination during the sample synthesis processes. In addition, Fig. 1S shows the narrow scan spectrum of Mg1s, Zn2p, Al2p, Ti2p, O1s and C1s in TiO_2/LDH-131 composites, respectively. It clearly find that the peak center of Zn2p, Al2p, and Ti2p were positioned at the binding energies of 1023.5, 74.63, 459.5 eV, respectively. Therefore, we can momentarily suggest that the oxidation states of Zn, Al, and Ti were Zn^{2+}, Al^{3+} and Ti^{4+} [34, 44].

3.1.6 UV–Vis DRS

Figure 7 displays UV–Vis DRS of the P25, TiO_2 and TiO_2/LDH-131 composites. The P25 nanoparticles presented a photoresponse with a wavelength in the areas of ultraviolet region since its large energy band gap (3.1 eV). After combining with the LDHs function materials, the TiO_2/

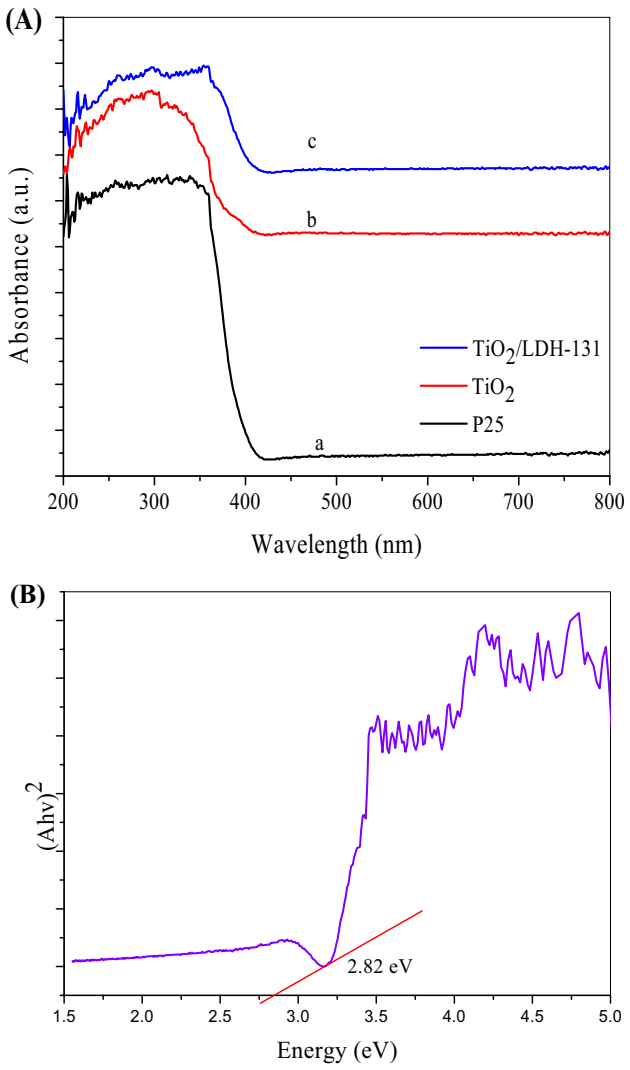

Fig. 7 **a** UV–Vis diffuse reflectance spectra of prepared-photocatalyst (*a*) P25, (*b*) TiO_2, (*c*) TiO_2/LDH-131 composites; **b** energy band gaps of TiO_2/LDH-131 composites

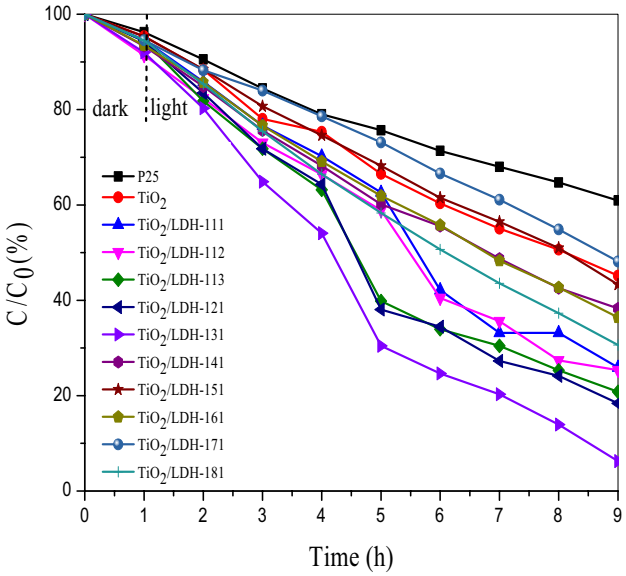

Fig. 8 Rhodamine B concentration as a function of time in different photocatalytic treatments. Reaction conditions: initial rhodamine B concentration of 10 mg/L, 50 mg photocatalyst, reaction temperature 25 ± 2 °C and initial pH 7.0

LDH-131 composites exhibited a red shift of light adsorption in the areas of visible light region, with the adsorption edges immediately broadening to about 440 nm. This is because that the visible-light-driven photocatalysts of LDHs hybrid materials and the fabrication of heterojunction composites between TiO_2 and LDHs generated a good photosensitizing effect [44]. Obviously, the light adsorption capacity of the TiO_2/LDH-131 composites gradually enhanced with the LDHs hybrid composites introducing, indicating the favorable responsiveness of the as-prepared samples to visible light. These encouraging results may be due to the introduction of LDHs hybrid materials and the BET surface area, which could affect the visible light adsorption and the generation and transfer of photoelectric electrons in the photocatalytic degradation process. Hence, the TiO_2/LDH composites could enhance the visible light adsorption ability, making those catalysts possible used in the visible-light-driven application.

3.2 Photocatalytic activity of the products

Figure 8 shows the photocatalytic degradation of rhodamine B over P25, TiO_2, and TiO_2/LDH composites under visible light irradiation. As for Fig. 8, we can see that the degradation rates of rhodamine B over P25 and TiO_2 nanoparticles was inappreciable, while the TiO_2/LDH composites presented conspicuous improved photocatalytic activities compared with P25 and TiO_2 nanoparticles. It may proved that the doped of TiO_2 nanoparticles and molar ratios of Mg, Zn and Al could observably affect the photocatalytic

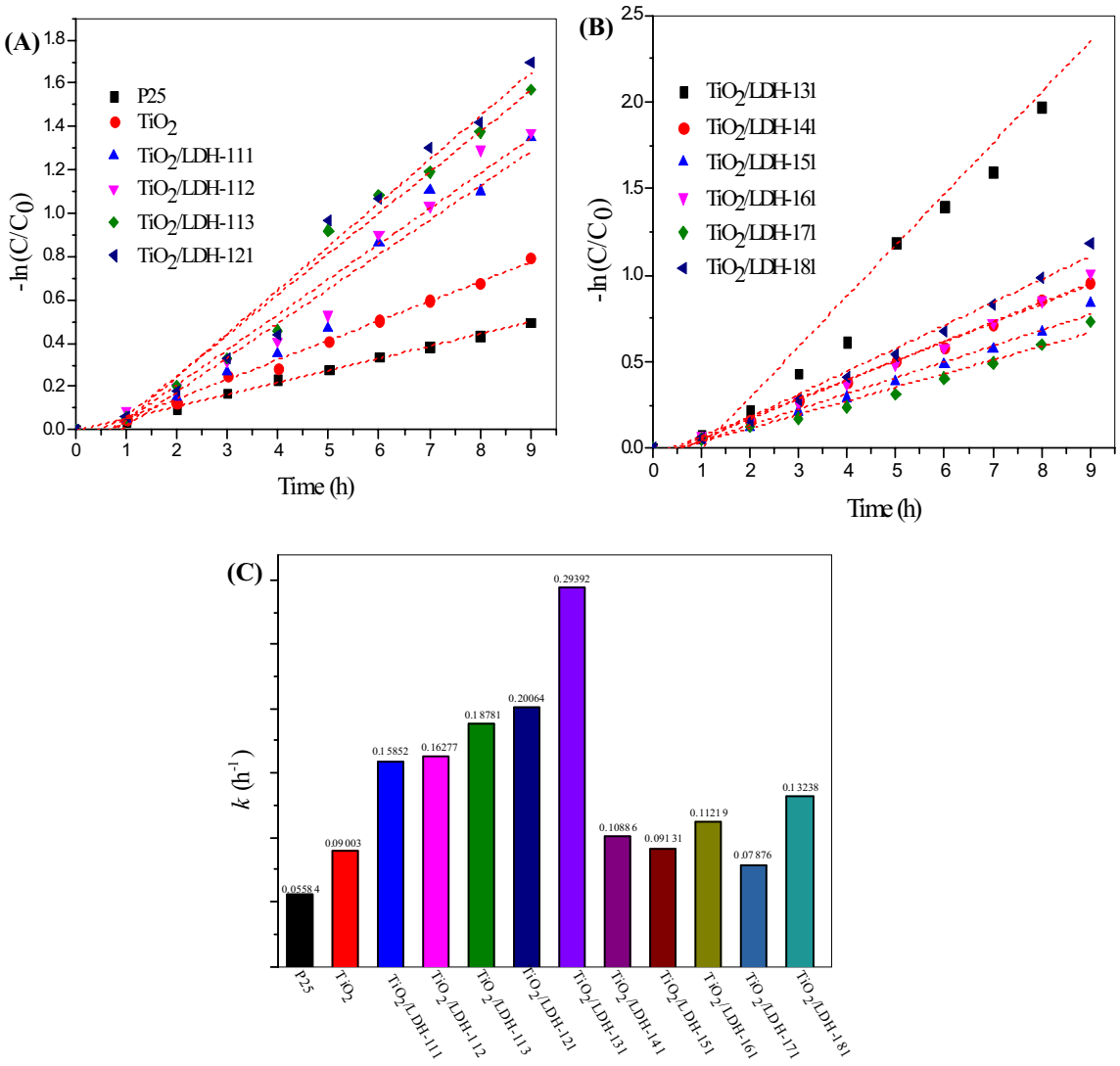

Fig. 9 **a, b** Pseudo-first-order degradation kinetics for rhodamine B with different photocatalysts, used to estimate Langmuir–Hinshelwood coefficients; **c** the rate constant k of rhodamine B with different photocatalysts

degradation activities of TiO_2/LDH composites. When the molar ratio of Zn atoms increased, the photocatalytic activity of TiO_2/LDH composites was accordingly enhanced gradually. But at the same time, with the molar ratio of Al atoms increasing, the photocatalytic activity of TiO_2/LDH composites was reducing inversely. Thus, the optimal molar ratio of TiO_2/LDH composites was 1:3:1. The TiO_2/LDH-131 composites exhibited the good activity with a degradation ratio of 93.73% after 8.0 h under visible light irradiation, while that over pure commercial P25 was only about 39.07%.

In order to investigate the photocatalytic decomposition kinetics behaviors of rhodamine B simulative dye wastewater, the experimental data corresponded to the Langmuir–Hinshelwood model, which could be studied by the following pseudo-first-order kinetics as the formula below (shown in Fig. 9a, b) [50, 51].

$$-\ln C/C_0 = k_a t \quad (1)$$

where, C_0 represents the original concentration of rhodamine B (mg/L), C is the concentration (mg/L) of rhodamine B at instantaneous time t, k_a and t stand for the apparent pseudo-first-order rated constant (h^{-1}) and time, respectively. The k_a of rhodamine B degradation in the photocatalytic process with P25 was 0.05584 h^{-1}, while that all TiO_2 (alkali treated P25) was only about 0.09003 h^{-1} as shown in Fig. 9C However, for the TiO_2/LDH composites, all of the apparent pseudo-first-order kinetic constants (k) had been enhanced than pure commercialized P25 powders. Comfortingly, as for the TiO_2/LDH-131 composites, its apparent pseudo-first-order kinetic constant k was up to 0.29392 h^{-1}, which was nearly 5.26 times and 3.26 times higher than those of pure P25 and TiO_2, respectively. The results indicated that the TiO_2/LDH composites have a good photocatalytic activity under visible light irradiation.

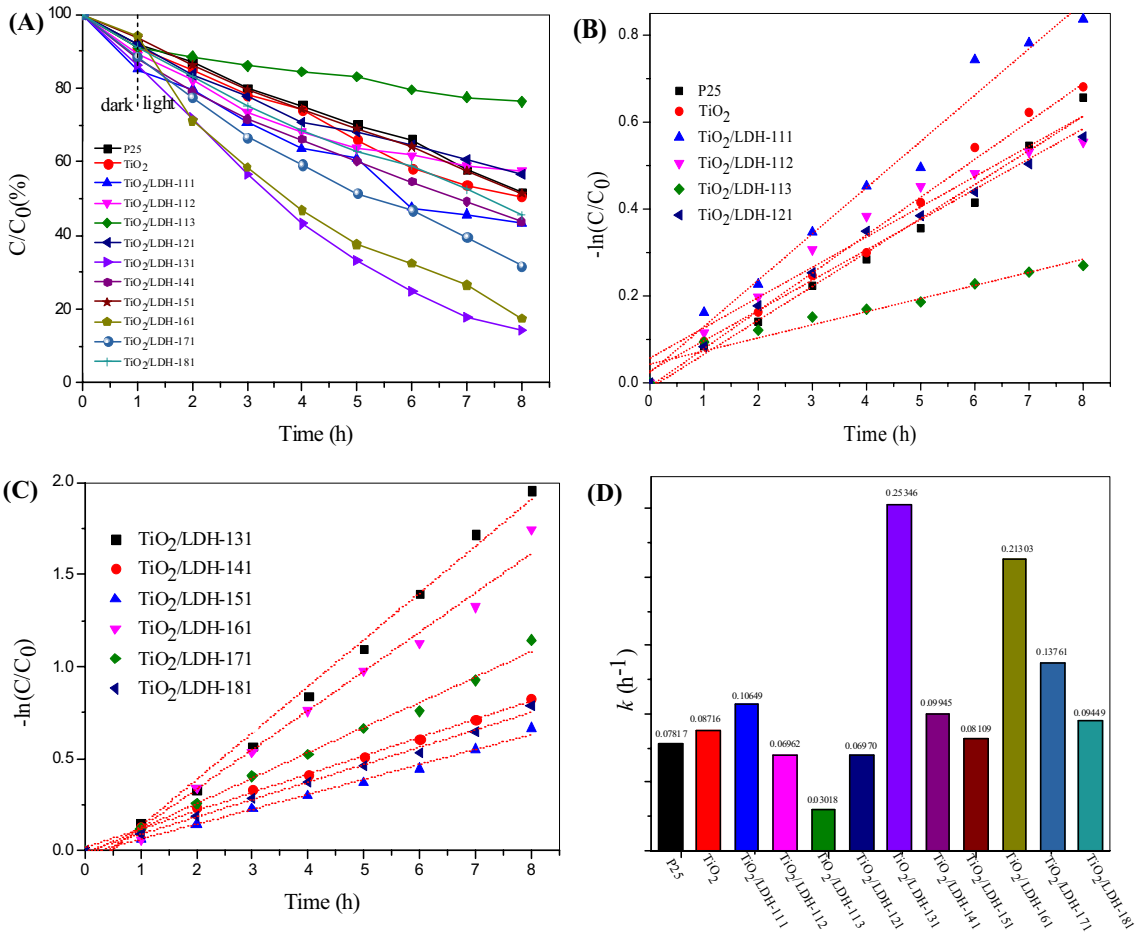

Fig. 10 **a** Methylene blue concentration as a function of time in different photocatalytic treatments. Reaction conditions: initial methylene blue concentration of 10 mg/L, 50 mg photocatalyst, reaction temperature 25 ± 2 °C and initial pH 7.0; **b, c** Pseudo-first-order degradation kinetics for methylene blue with different photocatalysts, used to estimate Langmuir–Hinshelwood coefficients; **d** the rate constant k of methylene blue with different photocatalysts

For the TiO_2/LDH composites prepared in this work, the TiO_2 combining with LDH composites would promote the photocatalytic activity as well as the separation efficiency of photoelectron transfer. Besides, as a distinguished photocatalyst, it is always wished to have high photocatalytic activity in degradation of different organic pollutants, then we also measured the ability of P25, TiO_2 and TiO_2/LDH composites in the degradation of methylene blue (MB) and the experimental results are located in Fig. 10. As shown Fig. 10, it is obvious that the degradation percentage of MB is 48.14, 49.39, 56.69, 42.54, 23.67, 43.24, 85.88, 56.23, 48.64, 82.51, 68.15 and 54.52% within 8.0 h over P25, TiO_2, TiO_2/LDH-111, TiO_2/LDH-112, TiO_2/LDH-113, and TiO_2/LDH-1b1 (b was 2–8), respectively, indicating that the composites have good photocatalytic activity, parts of composites have low photocatalytic activity in degradation of MB than pure P25 and TiO_2 nanoparticles. This is because that every catalyst has a specific surface area so that their adsorption capactivities are different. In addition, the difference of crystalline and catalyst active site of the prepared samples also can affect the photo-degradation activity. In a word, TiO_2/LDH-131 composites exhibited higher photocatalytic degradation activity than P25, TiO_2 and other composites.

4-Nitrophenol, one kind of phenolic organics, was chosen as a model pollutant to value the photocatalytic performance.

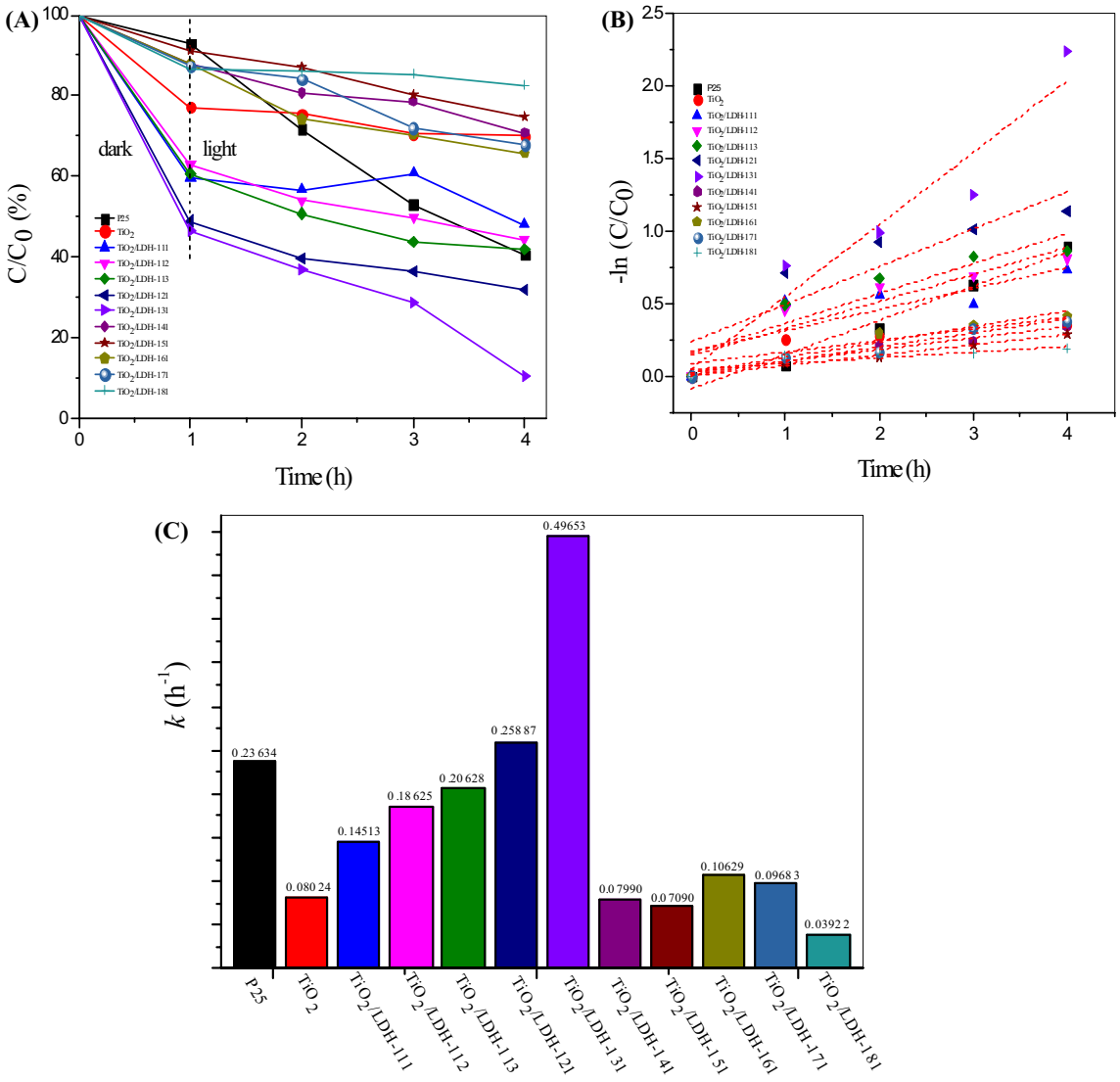

Fig. 11 **a** 4-Nitrophenol concentration as a function of time in different photocatalytic treatments. Reaction conditions: initial 4-nitrophenol concentration of 4 mg/L, 50 mg photocatalyst, reaction temperature 25 ± 2 °C and initial pH 7.0; **b** Pseudo-first-order degradation kinetics for 4-nitrophenol with different photocatalysts, used to estimate Langmuir–Hinshelwood coefficients; **c** the rate constant k of 4-nitrophenol with different photocatalysts

As shown in Fig. 11, TiO_2/LDH-131 composites still showed higher photocatalytic activity than commercial P25, pure TiO_2 and other prepared photocatalysts. As found in Fig. 11, 59.37, 30.00, 51.99, 55.71, 57.98, 68.18, 89.33, 29.15, 25.24, 34.20, 32.09, and 17.29% of 4-nitrophenol were degraded by commercial P25, pure TiO_2, TiO_2/LDH-111, TiO_2/LDH-112, TiO_2/LDH-113, and TiO_2/LDH-1b1 (b was 2–8), respectively, showing that the composites have good photocatalytic activity. However, the photocatalytic activity of the photocatalysts was increased with the increasing of the Al atoms. Hence, the good activity of TiO_2/LDH-131 composites may be due to the well-uniform-dispersed structure and the relatively big surface than commercial P25 and pure TiO_2 nanoparticles, which was further proved by the SEM images.

3.3 Photocatalytic stability of products

Apart from photocatalytic activity, the stability and reusability of prepared catalysts are also key projects to their practical application [52]. The stability experiments of the as-obtained TiO_2/LDH-131 composites photocatalysts had been done under the same conditions. After finishing every photo-degradation process, collecting and recycling the used catalysts by centrifugation, washed them with absolute ethanol and distilled water in order to be reused in next cycle as previous reported [50]. As found in Fig. 12, after sixth consecutive runs of rhodamine B, methylene blue and 4-nitrophenol degradation, the photocatalytic activity of TiO_2/LDH-131 composites only exhibited a slight deactivation. Rather, the photocatalytic activity of TiO_2/LDH-131 composites still kept 80% of its original activity after being recycled for six times, indicating that the prepared TiO_2/LDH-131 composites possessed outstanding reusability and stability, and had potential practical application value in environmental purification.

3.4 Photocatalytic mechanism of photocatalysts

As shown in Fig. 13, the proposed possible mechanism of the degradation of rhodamine B, methylene blue and 4-nitrophenol by TiO_2/LDH-131 composites can be described as follows: first, on the surface of the TiO_2/LDH-131 composites, the photon of energy is equal to or greater than the band gap energy strikes. Then the electron valence band (VB) is promoted to the conduction band (CB), resulting in a continuous generation of holes in the valence band (h^+) and excess electrons in the conduction band (e^-). The details are as follow Eqs. [44, 53].

$$TiO_2/\text{LDH-131} \rightarrow TiO_2/\text{LDH-131}\left(h_{VB}{}^{+}\right) + TiO_2/\text{LDH-131}\left(e_{CB}{}^{-}\right) \quad (2)$$

Usually, the strong positive photogenerated holes (h^+) can be converted $^{\cdot}OH$ radicals by the water molecules adsorbed on its photocatalysts surface (Eq. 4) or by hydroxyl ions (Eq. 5), the $^{\cdot}OH$ radicals can subsequently oxidize the organic pollutants (Eqs. 6–9) [44, 54, 55].

$$TiO_2/\text{LDH-131}\left(h_{VB}{}^{+}\right) + H_2O_{ads} \rightarrow {}^{\cdot}OH + H^{+} \quad (3)$$

$$TiO_2/\text{LDH-131}\left(h_{VB}{}^{+}\right) + {}^{\cdot-}OH \rightarrow {}^{\cdot}OH \quad (4)$$

$$TiO_2/\text{LDH-131}\left(h_{VB}{}^{+}\right) + \text{rhodamine B} \rightarrow {}^{*}\text{rhodamine B} \quad (5)$$

$$TiO_2/\text{LDH-131}\left(h_{VB}{}^{+}\right) + \text{methylene blue} \rightarrow {}^{*}\text{methylene blue} \quad (6)$$

$$TiO_2/\text{LDH-131}\left(h_{VB}{}^{+}\right) + \text{4-nitrophenol} \rightarrow {}^{*}\text{4-nitrophenol} \quad (7)$$

$$^{\cdot}OH + {}^{*}\text{rhodamine B} \rightarrow \text{degradation product} \quad (8)$$

$$^{\cdot}OH + {}^{*}\text{methylene blue} \rightarrow \text{degradation product} \quad (9)$$

$$^{\cdot}OH + {}^{*}\text{4-nitrophenol} \rightarrow \text{degradation product} \quad (10)$$

On the other hand, the surface hydroxyl groups of the LDHs structure can react with the photogenerated holes in the VB of TiO_2 to consequently promote the production of ·OH [53].

In addition, the presence of oxygen in the CB of photocatalysts can generate a super-peroxide anion ($^{\cdot}O_2{}^{-}$) (Eq. 12), which can produce organic peroxide (Eqs. 13–15) and hydrogen peroxide (Eq. 16), and the hydrogen peroxide can also generate $^{\cdot}OH$ radicals (Eq. 17) [44].

$$TiO_2/\text{LDH-131}\left(e_{CB}{}^{-}\right) + O_2 \rightarrow \cdot O_2{}^{-} \quad (11)$$

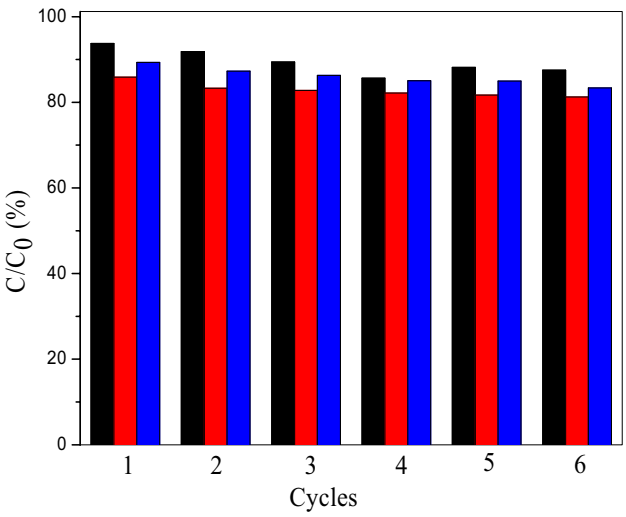

Fig. 12 Photocatalytic degradation cycle of rhodamine B, methylene B, and 4-nitrophenol on to TiO_2/LDH-131 composites

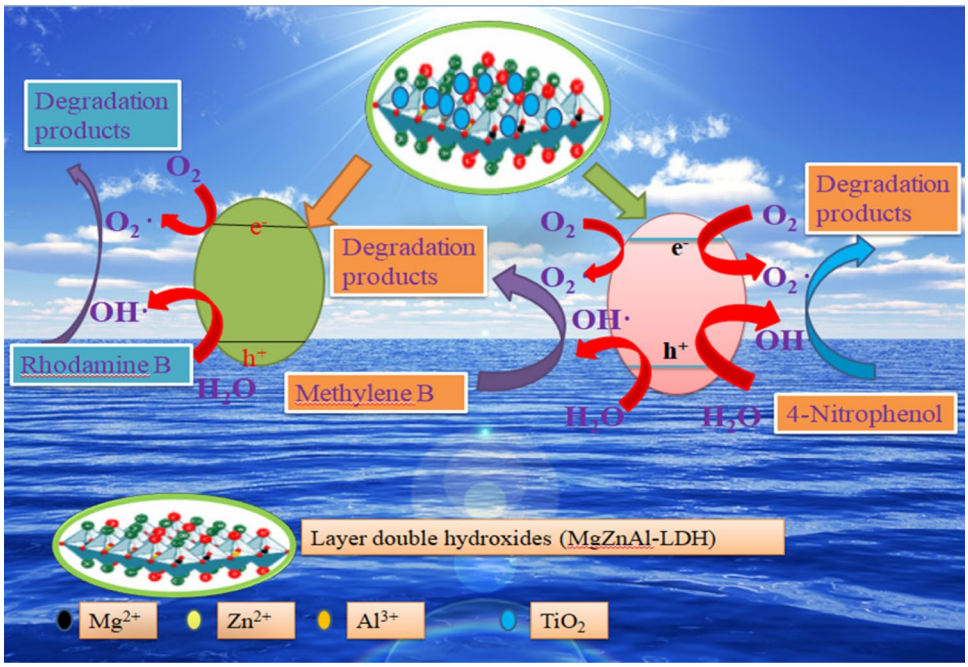

Fig. 13 Schematic diagram of the photocatalytic process occurring on the surface of the TiO_2/LDH composites

$$^{\cdot}O_2^- + \text{rhodamine B} \rightarrow \text{rhodamine B-OO}^{\cdot} \quad (12)$$

$$^{\cdot}O_2^- + \text{methylene blue} \rightarrow \text{methylene blue-OO}^{\cdot} \quad (13)$$

$$^{\cdot}O_2^- + \text{4-nitrophenol} \rightarrow \text{4-nitrophenol-OO}^{\cdot} \quad (14)$$

$$^{\cdot}O_2^- + HO_2^{\cdot} + H^+ \rightarrow H_2O_2 + O_2 \quad (15)$$

$$TiO_2/\text{LDH-131}\left(e_{CB}^-\right) + H_2O_2 \rightarrow {}^{\cdot}OH \quad (16)$$

Then, mounts of active species would react with rhodamine B, methylene blue, and 4-nitrophenol molecules to form harmless molecules. As shown in Fig. S2, the TOC removal ratio of rhodamine B, methylene blue, and 4-nitrophenol in 9.0, 8.0 and 4.0 h is 65.2, 61.3 and 63.4%, respectively. It is also implied that the mineralization is nearly completed. Comparing with other previous work, we can find that the TiO_2/LDH composites show satisfactory photocatalytic activities.

4 Conclusions

In this paper, typical TiO_2/LDH composites with different molar ratio of Mg, Zn, and Al atoms have been synthesized by a simple method. Series of characterizations proved that TiO_2/LDH composites are higher crystalline powders, having higher adsorption of visible light and more efficient separation of electron–hole pairs. Besides, the TiO_2/LDH composites used in UV–Vis photodegradation of rhodamine B, methylene blue, and 4-nitrophenol in aqueous solution revealed high photocatalytic activity. In comparison with commercial P25, pure nanoparticles, TiO_2/LDH composites, TiO_2/LDH-131 composites displayed good photocatalytic efficiency for the photodegradation of rhodamine B, methylene blue, and 4-nitrophenol organic pollutants under visible light irradiation. Furthermore, the degradation ratios of rhodamine B, methylene blue, and 4-nitrophenol are still more than 80% after six cycle runs. At the same time, the possible mechanisms and synthetic conditions of the reported could be easily extended to synthesize other materials for different applications.

Acknowledgements The authors would like to thank National Natural Science Foundation of China (Grant Nos. 21476269, 21776319), National College Students' Free Exploration Project of China (Grant No. 201710533255) and the Fundamental Research Funds for the Central Universities of Central South University (Grant No. 2017zzts777) for the financial supports of this work.

References

1. J.J. Sun, X.Y. Li, Q.D. Zhao, M.O. Tadé, S.M. Liu, Construction of p-n heterojunction β-Bi_2O_3/$BiVO_4$ nanocomposite with improved photoinduced charge transfer property and enhanced activity in degradation of ortho-dichlorobenzene. Appl. Catal. B **219**, 259–268 (2017)
2. M.J. Tian, F. Liao, Q.F. Ke, Y.J. Gao, Y.P. Guo, Synergetic effect of titanium dioxide ultralong nanofibers and activated carbon fibers on adsorption and photodegradation of toluene. Chem. Eng. J. **328**, 962–976 (2017)
3. Y. Tang, G. Zhang, C. Liu, S. Luo, X. Xu, L. Chen, B. Wang, Magnetic TiO_2-graphene composite as a high-performance and recyclable platform for efficient photocatalytic removal of herbicides from water. J. Hazard. Mater. **252**, 115–122 (2013)

4. X. Chen, W.Y. Lu, T.F. Xu, N. Li, Z.X. Zhu, G.Q. Wang, W.X. Chen, Visible-light-assisted generation of high-valent iron-oxo species anchored axially on g-C_3N_4 for efficient degradation of organic pollutants. Chem. Eng. J. **328**, 853–861 (2017)
5. J.J. Lin, M.Q. Sun, X.W. Liu, Z.L. Chen, Functional kaolin supported nanoscale zero-valent iron as a Fenton-like catalyst for the degradation of Direct Black G. Chemosphere **184**, 664–672 (2017)
6. J.J. Xu, Y.M. Hu, C. Zeng, Y.H. Zhang, H.W. Huang, Polypyrrole decorated BiOI nanosheets: efficient photocatalytic activity for treating diverse contaminants and the critical role of bifunctional polypyrrol. J. Colloid Interference Sci. **505**, 719–727 (2017)
7. W. Somasiri, X.F. Li, W.Q. Ruan, C. Jian, Evolution of efficacy of up-flow anaerobic sludge blanket reactor in removal of colour and reduction of COD in real textile wastewater. Bioresour. Technol. **99**, 3692–3699 (2008)
8. Y. Areerob, K.Y. Cho, W.C. Oh, Microwave assisted synthesis of graphene-$Bi_8La_{10}O_{27}$-Zeolite nanocomposite with efficient photocatalytic activity towards organic dye degradation. J. Photochem. Photobiol. A **340**, 157–169 (2017)
9. F. Ansari, A. Sobhani, M. Salavati-Niasari, Green synthesis of magnetic chitosan nanocomposites by a new auto-combustion method. J. Magn. Magn. Mater. **410**, 27–33 (2016)
10. F. Ansari, A. Sobhani, M. Salavati-Niasari, $PbTiO_3$/$PbFe_{12}O_{19}$ nanocomposites: Green synthesis through an eco-friendly approach. Composites B **85**, 170–175 (2016)
11. F. Ansari, A. Sobhani, M. Salavati-Niasari, Facile synthesis, characterization and magnetic property of CuFe12O19 nanostructures via a sol-gel auto-combustion process. J. Magn. Magn. Mater. **401**, 362–369 (2016)
12. F. Ansari, A. Sobhani, M. Salavati-Niasari, Sol-gel auto-combustion synthesis of $PbFe_{12}O_{19}$ using maltose as a novel reductant. RSC Adv. **4**, 63946–63950 (2014)
13. M. Panahi-Kalamuei, M. Mousavi-Kamazani, M. Salavati-Niasari, Facile hydrothermal synthesis of tellurium nanostructures for solar cells. J. Nanostruct. **4**, 459–465 (2014)
14. F. Beshkar, M. Salavati-Niasari, Facile synthesis of nickel chromite nanostructures by hydrothermal route for photocatalytic degradation of acid black 1 under visible light. J. Nanostruct. **5**, 17–23 (2015)
15. L. Nejati-Moghadam, A.E. Bafghi-Karimabad, M. Salavati-Niasari, H. Safardoust, Synthesis and characterization of SnO_2 nanostructures prepared by a facile precipitation method. J. Nanostruct. **5**, 47–53 (2015)
16. S.T. Fardood, Z. Golfar, A. Ramazani, Novel sol-gel synthesis and characterization of superparamagnetic magnesium ferrite nanoparticles using tragacanth gum as a magnetically separable photocatalyst for degradation of reactive blue 21 dye and kinetic study. J. Mater. Sci. **28**, 172002–172008 (2017)
17. F. Chen, Q. Yang, F.B. Yao, S.N. Wang, J. Sun, H.X. An, K.X. Yi, Y.L. Wang, Y.Y. Zhou, L.L. Wang, X.M. Li, D.B. Wang, G.M. Zeng, Visible-light photocatalytic degradation of multiple antibiotics by AgI nanoparticle-sensitized Bi5O7I microspheres: Enhanced interfacial charge transfer based on Z-scheme heterojunctions. J. Catal. **352**, 160–170 (2017)
18. E.S. Mehr, M. Sorbiun, A. Ramazani, S.T. Fardood, Plant-mediated synthesis of zinc oxide and copper oxide nanoparticles by using ferulago angulata (schlecht) boiss extract and comparison of their photocatalytic degradation of Rhodamine B (RhB) under visible light irradiation. J. Mater. Sci. **29**, 1333–1340 (2018)
19. L.L. Wang, X. Liu, J.M. Luo, X.D. Duan, J. Crittenden, C.B. Liu, S.Q. Zhang, Y. Pei, Y.X. Zeng, X.F. Duan, Self-optimization of the active site of molybdenum disulfide by an irreversible phase transition during photocatalytic hydrogen evolution. Angew. Chem. Int. Ed. **56**, 7610–7614 (2017)
20. S. Kumar, A. Kumar, Enhanced photocatalytic activity of rGO-CeO_2 nanocomposites driven by sunlight. Mater. Sci. Eng. B **223**, 98–108 (2017)
21. S.T. Fardood, A. Ramazani, S. Moradi, Green synthesis of Ni-Cu-Mg ferrite nanoparticles using tragacanth gum and their use as an efficient catalyst for the synthesis of polyhydroquinoline derivatives. J. Sol Gel Sci. Technol. **82**, 432–439 (2017)
22. S.T. Fardood, A. Ramazani, S. Moradi, P.A. Asiabi, Green synthesis of zinc oxide nanoparticles using Arabic gum and photocatalytic degradation of direct blue 129 dye under visible light. J. Mater. Sci. **28**, 13596–13601 (2017)
23. S.T. Fardood, A. Ramazani, S. Moradi, A novel green synthesis of nickel oxide nanoparticles using Arabic gum. Chem. J. Mold. **12**, 115–118 (2017)
24. A. Fujishima, K. Honda, Electrochemical photolysis of water at a semiconductor electrode. Nature **238**, 37–38 (1972)
25. U. Alam, M. Fleisch, I. Kretschmer, D. Bahnemann, M. Muneer, One-step hydrothermal synthesis of Bi-TiO_2 nanotube/graphene composites: an efficient photocatalyst for spectacular degradation of organic pollutants under visible light irradiation. Appl. Catal. B **218**, 758–769 (2017)
26. Y. Zhou, Y.W. Wu, Y.H. Li, Y.H. Liu, L.Y. Yang, L.P. Wang, H. Liu, D.D. Li, Q.S. Luo, The synthesis of 3D urchin-like TiO_2-reduced grapheme micro/nano structure composite and its enhanced photocatalytic properties. Ceram. Int. **42**, 12482–12489 (2016)
27. M. Dadkhah, M. Salavati-Niasari, N. Mir, Synthesis and characterization of TiO_2 nanoparticles by using new shape controllers and its application in dye sensitized solar cells. J. Ind. Eng. Chem. **20**, 4039–4044 (2014)
28. M. Sabet, M. Salavati-Niasari, Deposition of lead sulfide nanostructure films on TiO_2 surface via different chemical methods due to improving dye-sensitized solar cells efficiency. Electrochim. Acta. **169**, 168–179 (2015)
29. K. Wenderich, G. Mul, Methods, mechanism, and applications of photodeposition in photocatalysis: a review. Chem. Rev. **116**, 14587–14619 (2016)
30. S. Khanchandani, S. Kumar, A.K. Ganguli, Comparative study of TiO_2/CuS core/shell and composite nanostructures for efficient visible light photocatalysis. ACS Sustain. Chem. Eng. **4**, 1487–1499 (2016)
31. S.Y. Pu, R.X. Zhu, H. Ma, D.L. Deng, X.J. Pei, F. Qi, W. Chu, Facile in-situ design strategy to disperse TiO_2 nanoparticles on grapheme for the enhanced photocatalytic degradation of rhodamine 6G. Appl. Catal. B **218**, 208–219 (2017)
32. Y. Zhang, J.R. Chen, L. Hua, S.J. Li, X.X. Zhang, W.C. Sheng, S.S. Cao, High photocatalytic activity of hierarchical SiO_2@C-doped TiO_2 hollow spheres in UV and visible light towards degradation of rhodamine B. J. Hazard. Mater. **340**, 309–318 (2017)
33. Y.Y. Wang, Y.Q. Zhang, Z.J. Liu, C. Xie, S. Feng, D.D. Liu, M.F. Shao, S.Y. Wang, Layered double hydroxide nanosheets with multiple vacancies obtained by dry exfoliation as highly efficient oxygen evolution electrocatalysts. Angew. Chem. Int. Ed. **56**, 5867–5871 (2017)
34. Q. Wang, D. O'Hare, Recent advances in the synthesis and application of layered double hydroxide (LDH) nanosheets. Chem. Rev. **112**, 4124–4155 (2012)
35. K. Teramura, S. Iguchi, Y. Mizuno, T. Shishido, T. Tanaka, Photocatalytic conversion of CO_2 in water over layered double hydroxides. Angew. Chem. Int. Ed. **51**, 8008–8011 (2012)
36. Y.M.H. Zhou, L. Shuai, X.Y. Jiang, F.P. Jiao, J.G. Yu, Visible-light-driven photocatalytic properties of layered double hydroxide supported-Bi_2O_3 modified by Pd(II) for methylene blue. Adv. Powder Technol. **26**, 439–447 (2015)

37. W.L. Qin, H. Lv, T. Xia, Y. Ye, X.G. Chen, S.S. Lyu, TiO_2 intercalated talc nanocomposite: Preparation, characterization, and its photocatalytic performance. J. Nanosci. Nanotechnol. **17**, 6558–6565 (2017)
38. W.Y. Hernández, F. Alic, A. Verberckmoes, P.V.D. Voort, Tuning the acidic-basic properties by Zn-substitution in Mg-Al hydroxides as optimal catalysts for the aldol condensation reaction. J. Mater. Sci. **52**, 628–642 (2017)
39. M. Mureseanu, T. Radu, R.D. Andrei, M. Darie, G. Carja, Green synthesis of g-C_3N_4/CuONP/LDH composites and derived g-C_3N_4/MMO and their photocatalytic performance for phenol reduction from aqueous solutions. Appl. Clay Sci. **141**, 1–12 (2017)
40. X. Wu, D. Zhang, F.P. Jiao, S. Wang, Visible-light-driven photodegradation of methyl orange using Cu_2O/ZnAl calcined layered double hydroxides as photocatalysts. Colloid Surf. A **508**, 110–116 (2016)
41. X. Chen, H.K. Li, H.S. Wu, Y.X. Wu, Y.Y. Shang, J. Pan, X. Xiong, Fabrication of TiO_2@PANI nanobelts with the enhanced absorption and photocatalytic performance under visible light. Mater. Lett. **172**, 52–55 (2016)
42. S.F. Kang, H.F. Qin, L. Zhang, Y.K. Huang, X. Bai, X. Li, D. Sun, Y.G. Wang, L.F. Cui, Efficient photocatalytic bilirubin removal over the biocompatible core/shell P25/g-C_3N_4 heterojunctions with metal-free exposed surfaces under moderate green light irradiation. Sci. Rep. **7**, 44338–44348 (2017)
43. Y. Zhou, Y.W. Wu, Y.H. Li, Y.H. Liu, L.Y. Yang, L.P. Wang, H. Liu, D.D. Li, Q.S. Luo, The synthesis of 3D urchin-like TiO_2-reduced graphene micro/nano structure composite and its enhanced photocatalytic properties. Ceram. Int. **42**, 12482–12489 (2016)
44. M.F.D. Almeida, C.R. Bellato, A.H. Mounteer, S.O. Ferreira, J.L. Milagres, L.D.L. Miranda, Enhanced photocatalytic activity of TiO_2-impregnated with MgZnAl mixed oxides obtained from layered double hydroxides for phenol degradation. Appl. Surf. Sci. **357**, 1765–1775 (2015)
45. C. Ma, F.H. Wang, C. Zhang, Z.G. Yu, J.J. Wei, Z.Z. Yang, Y.Q. Li, Z.H. Li, M.Y. Zhu, L.Q. Shen, G.M. Zeng, Photocatalytic decomposition of Congo red under visible light irradiation using MgZnCr-TiO_2 layered double hydroxide. Chemosphere. **168**, 80–90 (2017)
46. B. Sun, G.W. Zhou, T.T. Gao, H.J. Zhang, H.H. Yu, NiO nanosheet/TiO_2 nanorods-constructed p-n heterostructures for improved photocatalytic activity. Appl. Surf. Sci. **364**, 322–331 (2016)
47. F. Ansari, F. Soofivand, M. Salavati-Niasari, Utilizing maleic acid as a novel fuel for synthesis of $PbFe_{12}O_{19}$ nanoceramics via sol-gel auto-combustion route. Mater. Charact. **103**, 11–17 (2015)
48. F. Ansari, M. Salavati-Niasari, Simple sol-gel auto-combustion synthesis and characterization of lead hexaferrite by utilizing cherry juice as a novel fuel and green capping agent. Adv. Powder Technol. **27**, 2025–2031 (2016)
49. F. Ansari, M. Bazarganipour, M. Salavati-Niasari, $NiTiO_3$/$NiFe_2O$ nanocomposites: Simple sol-gel auto-combustion synthesis and characterization by utilizing onion extract as a novel fuel and green capping agent. Mater. Sci. Semicond. Proc. **43**, 34–40 (2016)
50. G.Q. Zhao, C.F. Li, X. Wu, J.G. Yu, X.Y. Jiang, W.J.H. Hu, F.P. Jiao, Reduced graphene oxide modified NiFe-calcinated layered double hydroxides for enhanced photocatalytic removal of methylene blue. Appl. Surf. Sci. **434**, 251–259 (2018)
51. G.Q. Zhao, D. Zhang, J.G. Yu, Y. Xie, W.J.H. Hu, F.P. Jiao, Multi-walled carbon nanotubes modified Bi_2S_3 microspheres for enhanced photocatalytic decomposition efficiency. Ceram. Int. **43**, 15080–15088 (2017)
52. C.S. Zhu, J.T. Zheng, L.Y. Fang, P. Hu, Y.K. Liu, X.Q. Cao, M.B. Wu, Advanced visible-light driven photocatalyst with enhanced charge separation fabricated by facile deposition of Ag_3PO_4 nanoparticles on grapgene-like *h*-BN nanosheets. J. Mol. Catal. A **424**, 135–144 (2016)
53. V. Iliev, D. Tomova, L. Bilyarska, A. Eliyas, L. Petrov, Photocatalytic properties of TiO_2 modified with platinum and silver nanoparticles in the degradation of oxalic acid in aqueous solution. Appl. Catal. B **63**, 266–271 (2006)
54. L.Y. Chai, Q.W. Wang, Q.Z. Li, Z.H. Yang, Y.Y. Wang, Enhanced removal of Hg (II) from acidic aqueous solution using thiol-functionalized biomass. Water Sci. Technol. **62**, 2157–2166 (2010)
55. M. Hadnadjev-Kostic, T. Vulic, R. Marinkovic-Neducin, Solar light induced rhodamine B degradation assisted by TiO_2-Zn-Al LDH based photocatalysts. Adv. Powder Technol. **25**, 1624–1633 (2014)